

Computation-Guided Design of a Stimulus-Responsive Multienzyme Supramolecular Assembly

Lu Yang,^[a, d] Elliott M. Dolan,^[a, d] Sophia K. Tan,^[d] Tianyun Lin,^[d] Eduardo D. Sontag,^[c, d, e] and Sagar D. Khare^{*[a, b, c, d]}

Many enzymes in cells form multienzyme complexes, bringing their active sites in close proximity to each other in a spatio-temporally regulated manner. Enzyme clustering can lead to higher metabolic flux as a result of substrate channeling, sequestration of toxic intermediates, and decreased competing side reactions.^[1–5] Based on this natural blueprint, the design of artificial multienzyme metabolons has been attempted both in vitro and in vivo by using a host of colocalization strategies.^[6–14] Although these strategies were successful in improving the efficiency of synthetic metabolic pathways to various extents, no temporal control, which is characteristic of natural metabolic assemblies, such as the purinosome,^[15] on the formation of the multienzyme complexes has been designed. The ability to control synthetic metabolic pathways by using external stimuli, such as phosphorylation, light, pH and temperature, would afford precise temporal control over synthetic pathway flux and dynamics.^[2] A modular design approach for introducing stimulus responsiveness would allow a plug-and-play framework, in which any chosen multienzyme pathway could be made responsive to multiple chosen stimuli. We therefore developed a scaffold-free, modular design approach for using phosphorylation and light to trigger the formation of a multienzyme assembly.

As a model system, we considered a synthetic metabolic pathway, composed of three enzymes, for the degradation of the toxic groundwater pollutant 1,2,3-trichloropropane (TCP) to the benign product glycerol (GLY), which has been previous-

ly assembled, both in vivo and in vitro.^[16–20,21] Three pathway enzymes, haloalkane dehalogenase (DhaA), haloalcohol dehalogenase (HheC) and epoxide hydrolase (EchA), convert TCP to GLY in five steps (Figure 1A). We used a variant haloalkane dehalogenase DhaA31, which is approximately 30 times more efficient than the wild-type DhaA^[22] in catalyzing TCP hydrolysis, and wild-type EchA and HheC enzymes as our design starting points. Phosphorylation control on multienzyme assembly formation was achieved by fusing a previously engineered phosphotyrosine-binding Src homology 2 (SH2) domain^[23] and its corresponding phosphorylatable binding peptide to DhaA31 and HheC, respectively. Optical control over enzyme localization was realized by developing a structure-guided, computationally designed Src homology 3 (SH3) domain that could covalently crosslink with methionine on its corresponding peptide under 350 nm UV light (Figure 1B). We used computational simulations to construct atomic-resolution models of the designed synthetic metabolons to evaluate sites of fusion structures and to resolve the relative locations of active sites as well as the geometric compatibility of the resulting inter-enzyme connections.

Five different SH2 domain–DhaA31 fusions (see Section S2 in the Supporting Information) were modeled, and the binding partner peptide GEPQEEI was fused at the C-terminal end of HheC via a glycine-serine (GS)-rich linker. Computational modeling, performed by using Monte Carlo conformation sampling simulations implemented with Rosetta software showed that, among the five different fusions, the construct with the SH2 domain fused to the N terminus of DhaA31 with a flexible linker gave the lowest energy distribution for this two-component assembly (Figure S1 in the Supporting Information). This analysis also demonstrated that the addition of the SH2 domain at the N terminus of DhaA31 and the binding peptide at the C terminus of HheC allowed the active sites to be placed within 5–10 nm of each other, and enabled the formation of a contiguous surface linking the two active sites in low-energy conformations (Figure 2A, B). We hypothesized that if these low-energy conformations are significantly populated, enzyme co-localization and substrate channeling between the two active sites, including by bounded diffusion on the contiguous surface, might occur.^[9,24–28] Enhanced transfer of the intermediate, 2,3-dichloropropane-1-ol (DCP), to the HheC active site would result in a lower apparent value for the Michaelis constant, K_m , for HheC, and might lead to an improvement in pathway flux. Therefore, we chose N-terminally fused SH2 domain (SH2-DhaA31, hereafter) for use in the assemblies.

Both fusion enzymes, SH2-DhaA31 and HheC-sh2tag (HheC fused at its C-terminal end to the binding peptide for the SH2

[a] L. Yang, E. M. Dolan, Prof. Dr. S. D. Khare
Department of Chemistry and Chemical Biology
Rutgers, The State University of New Jersey
Piscataway, NJ 08854 (USA)
E-mail: sagar.khare@rutgers.edu

[b] Prof. Dr. S. D. Khare
Computational Biology & Molecular Biophysics Program
Rutgers, The State University of New Jersey
Piscataway, NJ 08854 (USA)

[c] Prof. Dr. E. D. Sontag, Prof. Dr. S. D. Khare
Institute for Quantitative Biomedicine
Rutgers, The State University of New Jersey
Piscataway, NJ 08854 (USA)

[d] L. Yang, E. M. Dolan, S. K. Tan, T. Lin, Prof. Dr. E. D. Sontag,
Prof. Dr. S. D. Khare
Center for Integrative Proteomics Research
Rutgers, The State University of New Jersey
Piscataway, NJ 08854 (USA)

[e] Prof. Dr. E. D. Sontag
Department of Mathematics, Rutgers, The State University of New Jersey
Piscataway, NJ 08854 (USA)

Supporting information and the ORCID identification numbers for the authors of this article can be found under <https://doi.org/10.1002/cbic.201700425>.

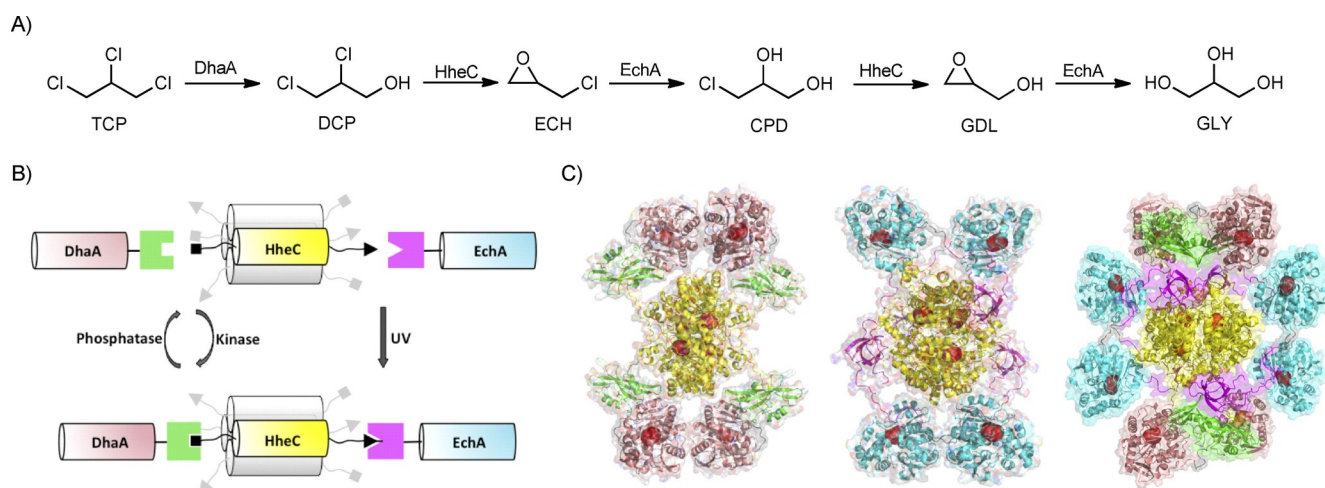


Figure 1. A) Synthetic pathway for the biodegradation of 1,2,3-trichloropropane. B) Schematic of the designed multienzyme assembly controlled by both phosphorylation and UV light. C) Illustration of designed multienzyme metabolons (active sites highlighted in red). Left: DhaA–HheC two-component assembly; center: HheC–EchA two-component assembly; right: DhaA–HheC–EchA three-component assembly.

domain), were expressed in *Escherichia coli* and purified by standard Ni-NTA chromatography. At the concentration used for generating assemblies, SH2-DhaA31 was marginally worse than DhaA31 in catalyzing the conversion of TCP to DCP, whereas HheC-sh2tag was as active as wild-type HheC (Figure S2); this indicated that the constructing fusions had no significant negative effect on the activity of either enzyme. The measured binding affinity between SH2-DhaA31 and HheC-pYsh2tag (dissociation constant, $K_d = 43 \pm 7$ nM) was moderately weaker (\approx tenfold) than the reported value for the free SH2 domain for the phosphopeptide^[23] (Figure S3), thus suggesting a small but measurable impact of enzyme fusion on affinity. Dynamic light scattering (DLS) and gel filtration chromatography (GFC) were used to characterize the formation and phosphorylation dependence of the two-enzyme assembly by using Src kinase and Lambda phosphatase. The observed increase (Figure 2C, D) and decrease (Figure S5) in the size of particles upon incubation with kinase and phosphatase enzymes, respectively, demonstrate that both assembly formation and disassembly can be controlled in a phosphorylation-dependent manner. Whereas DLS data showed the emergence of particles with a higher hydrodynamic radius upon phosphorylation (Figure 2C), GFC traces showed incomplete assembly formation, possibly as a result of dilution on the column (Figure 2D). However, increasing molar ratios (monomer/monomer) of DhaA/HheC led to species of higher apparent molecular weight (Figure 2D), indicating that assembly formation equilibria are dynamic and optimizable.

One-pot, two-enzyme conversion of TCP into epichlorohydrin (ECH) was investigated by measuring ECH using gas chromatography; the assembly showed a faster ECH production rate than a mixture of unassembled enzymes (Figure 2E). Numerical simulations based on Michaelis–Menten kinetics^[29] were performed to analyze this two-enzyme in-series reaction system (Section S6). We found that HheC is inhibited by its product and the ECH inhibition constant was, therefore, includ-

ed in the simulation (Figure S4). Simulated kinetics agree well with the experimental data obtained for both free enzymes and the assembly, and show that the assembled-enzyme system leads to an approximately threefold lower apparent K_m for HheC compared to the free-enzyme system (Figure 2E). Although structure-based conformational landscape mapping (Figure 2A, B) indicates that this decrease in apparent K_m might arise from the adoption of channeling-competent geometries in the lowest-energy conformers, proximity-based enhancement^[30] cannot be entirely ruled out without high-resolution structural characterization. To investigate the stimulus responsiveness of the designed assembly, we performed an experiment in which the SH2-DhaA31–HheC-sh2tag complex was assembled by using phosphorylation, and substrate TCP and free EchA were added at $t = 0$. At $t = 2$ hours, excess phosphatase or an equal volume of buffer was added to samples and controls, respectively. The observed decrease in the rate of GLY production after adding phosphatase compared to the controls shows that this two-enzyme system can be dynamically controlled in response to chosen external stimulus.

Having established a phosphorylation-mediated assembly between DhaA and HheC enzymes by using modular SH2-peptide interactions, we introduced UV-light-based control of multienzyme assembly by using similarly modular peptide-binding-domain interactions. We used *p*-benzoyl-L-phenylalanine (pBpa), an unnatural photoreactive amino acid that has been shown to participate in proximity-mediated covalent bioconjugation with proteins and peptides triggered by 350 nm UV light (Figure 3A).^[31–33] Based on the amino acid preferences and the mechanism of crosslinking of pBpa with C–H bonds,^[32] the Rosetta Enzyme Design approach^[34] was utilized to obtain a redesigned SH3 domain (PDB ID: 2O13) featuring a pBpa–methionine crosslink. Protein was expressed by using the pEvol system,^[33] and characterization of the binding properties of the isolated, redesigned SH3 domain showed that it was able to

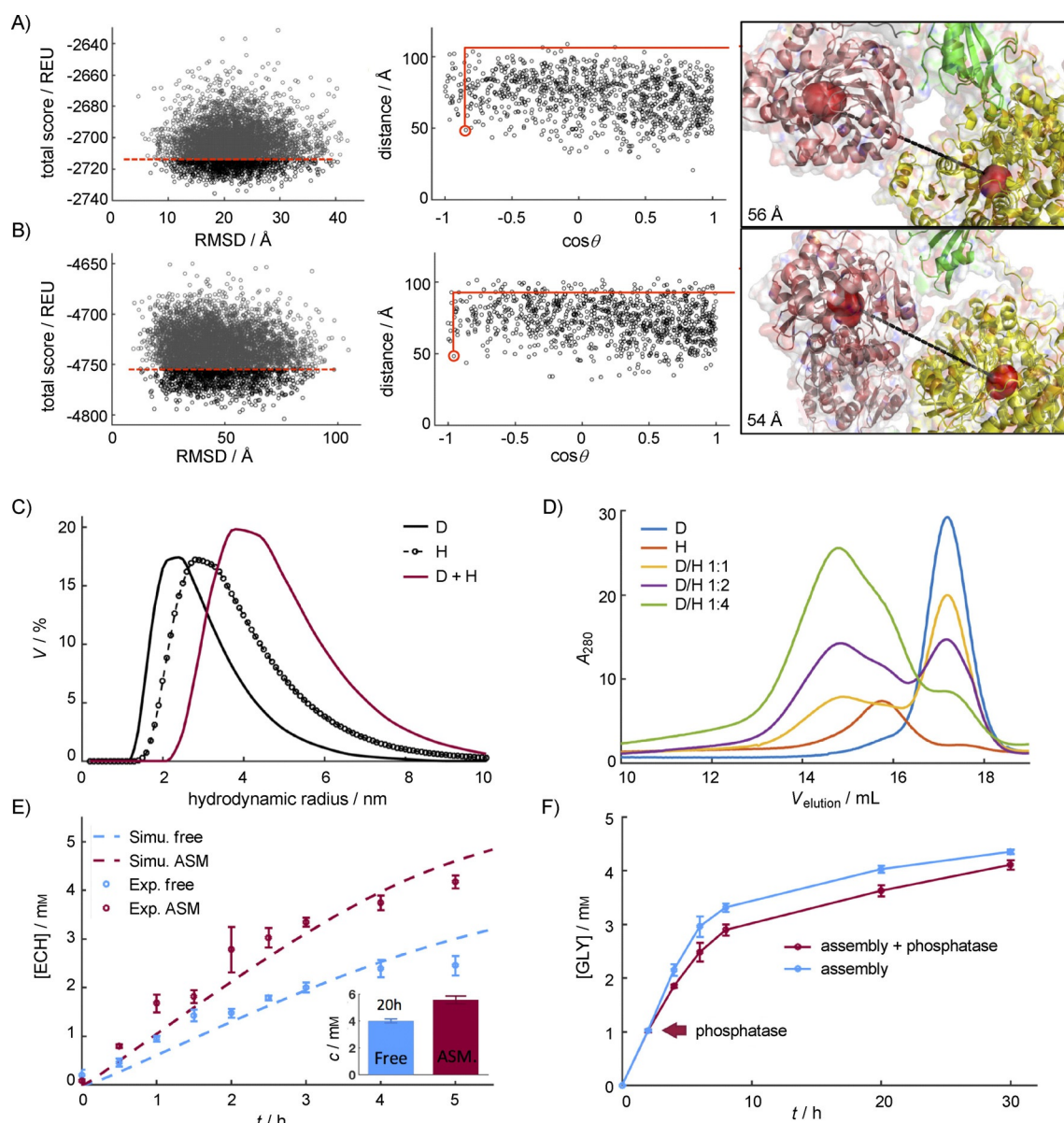


Figure 2. A) Asymmetric and B) Symmetric conformation simulation of the DhaA–HheC two-component assembly: Left: total score distribution in Rosetta energy units vs. RMSD; center: conformations with 20% lowest energy were used to analyze active-site distances and the orientation between active-site access tunnels; right: example structures (DhaA31: pink, SH2 domain: green, HheC: yellow). C) Volume distribution curves obtained from DLS of the SH2–DhaA31–HheC–pYsh2tag assembly formation. For DLS measurements, the sample concentration was 1 μM for both SH2–DhaA31 and HheC–pYsh2tag both as single components and in assembly. D) GFC elution profiles of single enzyme component 5 μM SH2–DhaA31, 5 μM HheC–pYsh2tag, and mixtures of the two at 1:1, 1:2, 1:4 ratios at a fixed concentration (5 μM) of SH2–DhaA31. E) Simulated and experimentally measured time courses of product ECH converted from 10 mM TCP. The bar graph shows TCP to ECH conversion after 20 h. F) TCP conversion activity by SH2–DhaA–HheC–pYsh2tag two-component assembly (1 μM :2 μM) and free EchA–SH3 (1 μM) with and without phosphatase (0.1 μM) added after 2 h, as determined by production of GLY. In all panels, D=SH2–DhaA31, H=HheC–pYsh2tag.

photo-crosslink covalently with its binding peptide upon exposure to 350 nm UV light (Figure S6).

The computationally designed pBpa-containing SH3 domain was fused to the C-terminus of EchA via a GS-rich linker, and the corresponding designed binding peptide (HSKYPLPLPSM) was fused to the N terminus of HheC-sh2tag via another GS-rich linker. Proteins were expressed and purified as described above, and the formation of a photo-crosslinked product between EchA-SH3 (44.8 kDa) and sh3tag-HheC-sh2tag (31.5 kDa) was observed by SDS-PAGE within two hours (Figure 3B). The

crosslinking efficiency was estimated to be $\approx 20\%$, which is not unlike previous reports in which incomplete crosslinking was observed.^[31] As the photo-crosslinking reaction is proximity mediated,^[32] crosslinking efficiency can be increased by designing a higher-affinity variant of the SH3–peptide interface. Nonetheless, these results indicate that our designed SH3 domain–peptide tag can be used to covalently crosslink cargo enzymes fused to them.

Despite the modest crosslinking efficiency observed, the yield of GLY (in four steps) from DCP after 12 h with the cross-

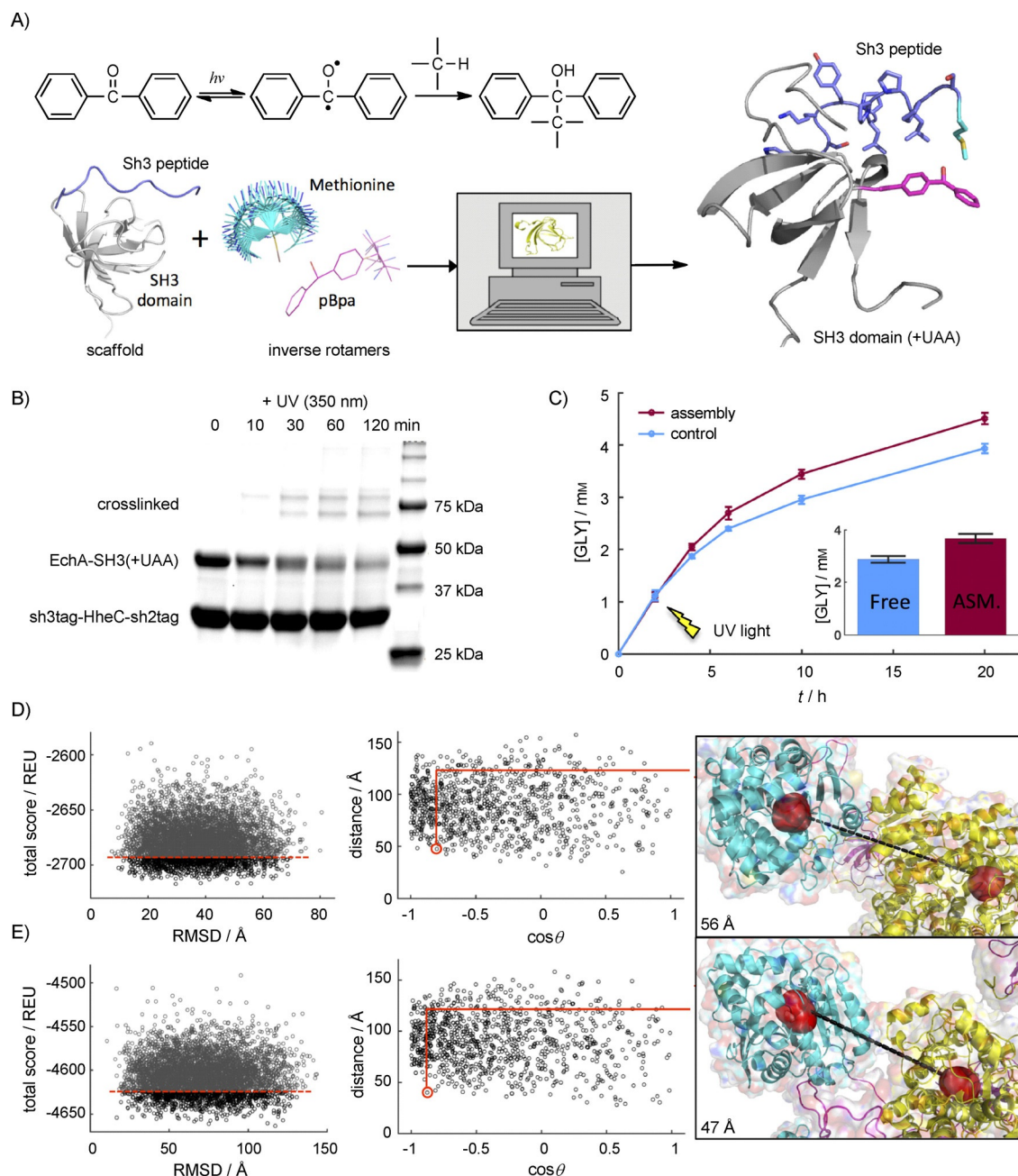


Figure 3. A) Schematic of the computational design approach. Design model highlighting the unnatural amino acid (UAA), *p*-benzoyl-L-phenylalanine, in the SH3 domain and methionine in the binding peptide. B) SDS-PAGE gel depicting the crosslinking between EchA-SH3 with UAA and sh3tag-HheC-sh2tag under 350 nm UV light irradiation for the indicated time intervals. C) DCP conversion activity was determined by measuring the concentration of GLY produced by assembly ($2 \mu\text{M}$ sh3tag-HheC-sh2tag and $1 \mu\text{M}$ EchA-SH3) and free enzymes ($2 \mu\text{M}$ wild-type HheC and $1 \mu\text{M}$ EchA-SH3). A 350 nm UV light stimulus was given at $t = 2$ h and lasted for 2 h. The bar graph shows GLY yield after 12 h with a preassembled sh3tag-HheC-sh2tag-EchA-SH3 two-enzyme assembly compared to free enzymes. D) Asymmetric and E) symmetric conformation simulation of the sh3tag-HheC-sh2tag-EchA-SH3 two-component assemblies.

linked enzymes was 28% higher than that of a control non-crosslinked enzyme mixture (Figures 3 C, inset, and S7). Photo-induced crosslinking was shown to be strictly dependent on the designed interaction between the SH3-domain and its binding tag fused to the HheC protein: no observable crosslinking between EchA-SH3 and the wild-type HheC or HheC-sh2tag variants (Figure S8) occurred. Furthermore, without crosslinking, no activity improvement was detectable (Figure S9). The stimulus responsiveness of the sh3tag-HheC-sh2tag-EchA-SH3 assembly was probed by shining 350 nm

light, for 2 h, after 2 h of addition of the substrate DCP to component enzymes, and, gratifyingly, a 14% increase in GLY production yield was obtained after 20 h, compared to the control (EchA-SH3 and wild-type HheC) in which no crosslinking was possible (Figure 3 C). To investigate the source of the observed increase in pathway efficacy, computational modeling (conformational sampling) was performed by using the same strategy as developed for the DhaA-HheC assembly. In the resulting landscape, we found that a majority of the distances between the mouths of the enzyme active-site tunnels are within

15 nm, and the angle between two enzyme active-site tunnel vectors (Section S2), a measure of the direction of the two active sites with respect to one another, showed a higher density towards 180°, thus indicating that, in the low-energy structures, the active sites are close to each other and are oriented favorably for metabolite channeling (Figure 3 D, E).

To combine the phosphorylation and UV-light-mediated colocalization, we mixed SH2-DhaA31, EchA-SH3 and sh3tag-HheC-sh2tag together, thus both SH2-DhaA31 and EchA-SH3

were expected to colocalize with the HheC tetramer upon phosphorylation and irradiation with UV light. A mixture of the three enzymes subjected to the two stimuli showed a larger hydrodynamic radius, based on DLS and GFC, than either two-enzyme assembly (Figures 4 A and S10). A comparison between TCP conversion activity catalyzed by 1) free enzymes, 2) SH2-DhaA31–HheCpYsh2tag assembly + free EchA-SH3, 3) free SH2-DhaA31 + sh3tag-HheC–EchA-SH3 assembly, and 4) the three-component assembly, showed that the three-component as-

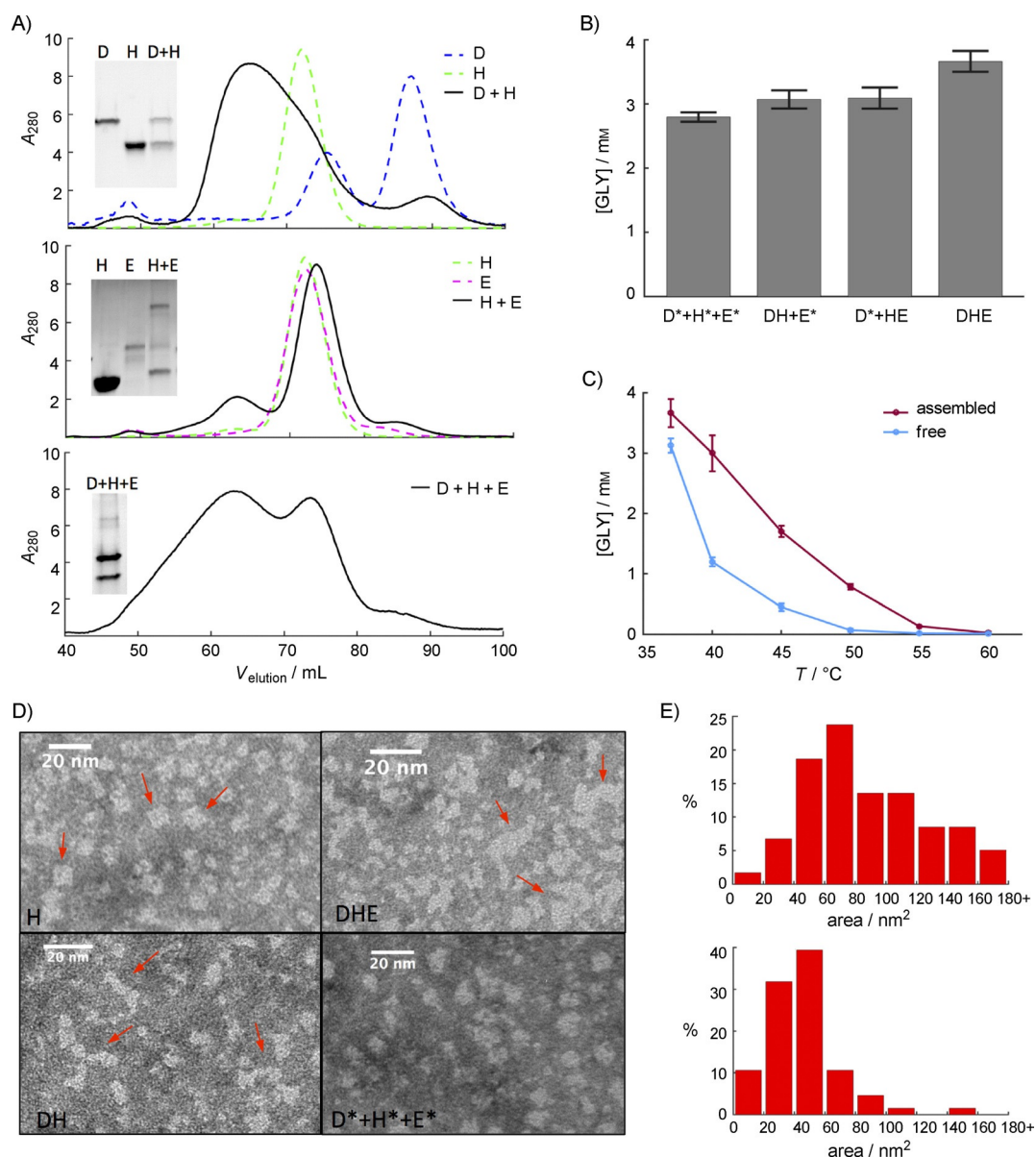


Figure 4. A) Gel filtration elution profiles of top: SH2-DhaA31, HheC-pYsh2tag and their mixture; middle: sh3tag-HheC-sh2tag–EchA-SH3 and their mixture after exposure to UV light; and bottom: the three-component assembly. Fractions from the main elution peaks were validated by SDS-PAGE (insets). B) TCP conversion activity determined by measuring GLY yield after 20 h. Different HheC variants 1) wild-type HheC, 2) HheC-pYsh2tag, 3) sh3tag-HheC-sh2tag, and 4) sh3tag-HheC-pYsh2tag were used along with the same SH2-DhaA31 and EchA-SH3 for TCP degradation to compare conversion efficiency among 1) free enzymes; 2) SH2-DhaA31–HheCpYsh2tag assembly + free EchA-SH3; 3) free SH2-DhaA31 + sh3tag-HheC-sh2tag–EchA-SH3 assembly; and 4) three-component assembly generated with phosphorylation and light, respectively. C) Thermotolerance profiles of the three-component assembly and free-enzyme mixture determined by residual activity (GLY yields after 20 h) after 30 min of exposure to the indicated temperatures. D) TEM images of top left: single sh3tag-HheC-sh2tag, bottom left: SH2-DhaA31–HheCpYsh2tag assembly, top right: three-component assembly, and bottom right: a mixture of free enzymes. E) ImageJ software was used to analyze size distribution in the micrographs for top: three-component assembly and bottom: the free enzyme mixture. In all figures D = SH2-DhaA, H = HheC-pYsh2tag (except B), E = EchA-SH3.

sembly had the highest conversion efficiency, whereas the free, unassembled enzymes gave the lowest conversion efficiency (Figures 4B and S11). The increase due to colocalization was insensitive to changes in the enzyme stoichiometry used for assembly, thus indicating that assembly formation was robust (Figure S12). To evaluate whether the colocalization of enzymes affords other functional benefits such as enhanced thermotolerance, an important parameter for the utility of synthetic metabolic pathways,^[6,24] we evaluated the ability of assembled enzymes and unassembled controls to tolerate a heat shock. GLY production yield at room temperature was measured after 30 min of exposure to a range of temperatures, and we found that the three-component assembly maintains activity to a greater extent than unassembled enzymes do (Figure 4C). Thus, apart from improvements in the pathway flux, the designed enzyme assembly also appears to impart greater robustness to harsher environments. Further engineering and optimization of assemblies for improving pathway activity at higher temperatures could benefit the use of these enzymes in wastewater treatment,^[16] and improvements in thermostability might be possible by the stabilization of the individual enzymes of the dehalogenation pathway.^[35]

Electron microscopy of assembled and unassembled enzymes was used to investigate the diversity of structures and structural changes upon assembly formation. Squares of 7–8 nm, presumably corresponding to the HheC tetramer, were the predominant species in the micrographs of single-component sh3tag-HheC-sh2tag (Figure 4D). The fraction of these squares decreased dramatically in micrographs of the two-component assembly, and several larger and elongated shapes were observed, thus indicating attachment of SH2-DhaA31 to HheC-sh2tag. The three-component assembly showed a highly diverse shape distribution, including structures that are significantly larger than those observed for the two-component assembly, as well as the shapes observed in a mixture of the three free enzymes (Figure 4E); this indicated that the designed interactions, and not nonspecific aggregation, are responsible for the detected shapes. Although the micrographs show that assemblies are formed as intended, the large size, polydispersity (partly due to low crosslinking efficiency), and conformational diversity of the assemblies precludes characterization of the observed structures by using higher-resolution techniques. Further computationally guided stabilization of the newly generated interfaces and replacement of GS-rich linkers with structured elements might aid in obtaining more uniform shapes and sizes that would be suitable for characterization by high-resolution structure-determination techniques.

In conclusion, we have demonstrated that a multistimulus-responsive multienzyme assembly has been built by using structure-guided and computationally designed modular protein-peptide interaction domains. Reversible and irreversible colocalization can be achieved by phosphorylation and UV photo-crosslinking, respectively. Both phosphorylation- and photo-crosslinking-driven two-enzyme systems showed improved reaction efficiency compared to non-crosslinked enzyme mixture controls, and the three-component assembly showed a further enhancement of product yields compared to

the two-enzyme assemblies. The magnitudes of increase in pathway efficacy were smaller compared to previous spatial-localization-based studies, which typically involve a reversible step so that colocalization has a large thermodynamic and kinetic boost.^[36] However, in contrast to colocalization with only spatial arrangement, the multistimulus-responsive enzyme-assembly approach provides temporal control and could be generally applicable to other pathway systems, including those with a reversible step. In vivo, temporal control over synthetic metabolic pathways should allow the levels of often toxic pathway intermediates to be regulated^[11,16]—thereby, making the process more efficient. Overall, we have shown that our approach for controllably constructing a multienzyme complex provides a viable methodology for artificial and dynamic metabolon design by using computational structure-based design approaches.

Acknowledgements

We thank Prof. Jiri Damborsky for donating plasmids harboring the genes for DhaA31, HheC and EchA, and Profs. Charles Dismukes, Vikas Nanda and Gaetano T. Montelione for access to instrumentation. We thank Prof. Peter Schultz for providing the pEvol-pBpa plasmid (Addgene).

Keywords: biodegradation · enzymes · photo-crosslinking · protein design · supramolecular enzyme assembly

- [1] I. Wheeldon, S. D. Minter, S. Banta, S. C. Barton, P. Atanassov, M. Sigman, *Nat. Chem.* **2016**, *8*, 299–309.
- [2] C. Schmidt-Dannert, F. Lopez-Gallego, *Microb. Biotechnol.* **2016**, *9*, 601–609.
- [3] R. J. Conrado, J. D. Varner, M. P. Delisa, W. Bentley, M. Betenbaugh, *Curr. Opin. Biotechnol.* **2008**, *19*, 492–499.
- [4] R. Chen, Q. Chen, H. Kim, K.-H. Siu, Q. Sun, S.-L. Tsai, W. Chen, *Curr. Opin. Biotechnol.* **2014**, *28*, 59–68.
- [5] H. Lee, W. C. DeLoache, J. E. Dueber, *Metab. Eng.* **2012**, *14*, 242–251.
- [6] X. Gao, S. Yang, C. Zhao, Y. Ren, D. Wei, *Angew. Chem. Int. Ed.* **2014**, *53*, 14027–14030; *Angew. Chem.* **2014**, *126*, 14251–14254.
- [7] O. I. Wilner, Y. Weizmann, R. Gill, O. Lioubashevski, R. Freeman, I. Willner, *Nat. Nanotechnol.* **2009**, *4*, 249–254.
- [8] J. E. Dueber, G. C. Wu, G. R. Malmirchegini, T. S. Moon, C. J. Petzold, A. V. Ullal, K. L. J. Prather, J. D. Keasling, *Nat. Biotechnol.* **2009**, *27*, 753–758.
- [9] J. Fu, M. Liu, Y. Liu, N. W. Woodbury, H. Yan, *J. Am. Chem. Soc.* **2012**, *134*, 5516–5519.
- [10] C. You, Y.-H. P. Zhang, *ACS Synth. Biol.* **2013**, *2*, 102–110.
- [11] J. V. Price, L. Chen, W. B. Whitaker, E. Papoutsakis, W. Chen, *Proc. Natl. Acad. Sci. USA* **2016**, *113*, 12691–12696.
- [12] F. Liu, S. Banta, W. Chen, *Chem. Commun.* **2013**, *49*, 3766.
- [13] Y. Liu, D. P. Hickey, J.-Y. Guo, E. Earl, S. Abdellaoui, R. D. Milton, M. S. Sigman, S. D. Minter, S. C. Barton, *ACS Catal.* **2017**, *7*, 2486–2493.
- [14] M. Park, Q. Sun, F. Liu, M. P. Delisa, W. Chen, D. F. Hozbor, *PLoS One* **2014**, *9*, e97103.
- [15] C. Y. Chan, H. Zhao, R. J. Pugh, A. M. Pedley, J. French, S. A. Jones, X. Zhuang, H. Jinnah, T. J. Huang, S. J. Benkovic, *Proc. Natl. Acad. Sci. USA* **2015**, *112*, 1368–1373.
- [16] P. Dvorak, S. Bidmanova, J. Damborsky, Z. Prokop, *Environ. Sci. Technol.* **2014**, *48*, 6859–6866.
- [17] T. Bosma, E. Kruijzinga, E. J. De Bruin, G. J. Poelarends, D. B. Janssen, *Appl. Environ. Microbiol.* **1999**, *65*, 4575–4581.
- [18] N. P. Kurumbang, P. Dvorak, J. Bendl, J. Brezovsky, Z. Prokop, J. Damborsky, *ACS Synth. Biol.* **2014**, *3*, 172–181.

- [19] T. Bosma, J. Damborský, G. Stucki, D. B. Janssen, *Appl. Environ. Microbiol.* **2002**, *68*, 3582–3587.
- [20] M. I. Arif, G. Samin, J. G. E. van Leeuwen, J. Oppentocht, D. B. Janssen, *Appl. Environ. Microbiol.* **2012**, *78*, 6128–6136.
- [21] P. Dvorak, L. Chrast, P. I. Nikel, R. Fedr, K. Soucek, M. Sedlackova, R. Chaloupkova, V. de Lorenzo, Z. Prokop, J. Damborsky, *Microb. Cell Fact.* **2015**, *14*, 201.
- [22] M. Pavlova, M. Klvana, Z. Prokop, R. Chaloupkova, P. Banas, M. Otyepka, R. C. Wade, M. Tsuda, Y. Nagata, J. Damborsky, *Nat. Chem. Biol.* **2009**, *5*, 727–733.
- [23] T. Kaneko, H. Huang, X. Cao, X. Li, C. Li, C. Voss, S. S. Sidhu, S. S. C. Li, *Sci. Signaling* **2012**, *5*, ra68.
- [24] Y.-H. P. Zhang, *Biotechnol. Adv.* **2011**, *29*, 715–725.
- [25] M. Pröschel, R. Detsch, A. R. Boccaccini, U. Sonnewald, *Front. Bioeng. Biotechnol.* **2015**, *3*, 168.
- [26] F. Lopez-Gallego, C. Schmidt-Dannert, *Curr. Opin. Chem. Biol.* **2010**, *14*, 174–183.
- [27] F. M. Raushel, J. B. Thoden, H. M. Holden, *Acc. Chem. Res.* **2003**, *36*, 539–548.
- [28] H. O. Spivey, J. Ovádi, *Methods* **1999**, *19*, 306–321.
- [29] P. Dvorak, N. P. Kurumbang, J. Bendl, J. Brezovsky, Z. Prokop, J. Damborsky, *ChemBioChem* **2014**, *15*, 1891–1895.
- [30] M. Castellana, M. Z. Wilson, Y. Xu, P. Joshi, I. M. Cristea, J. D. Rabinowitz, Z. Gitai, N. S. Wingreen, *Nat. Biotechnol.* **2014**, *32*, 1011–1018.
- [31] J. C. Kauer, S. Erickson-Viitanen, H. R. Wolfe, W. F. DeGrado, *J. Biol. Chem.* **1986**, *261*, 10695–10700.
- [32] A. Wittelsberger, B. E. Thomas, D. F. Mierke, M. Rosenblatt, *FEBS Lett.* **2006**, *580*, 1872–1876.
- [33] J. W. Chin, A. B. Martin, D. S. King, L. Wang, P. G. Schultz, *Proc. Natl. Acad. Sci. USA* **2002**, *99*, 11020–11024.
- [34] F. Richter, A. Leaver-Fay, S. D. Khare, S. Bjelic, D. Baker, *PLoS One* **2011**, *6*, e19230.
- [35] D. Bednar, K. Beerens, E. Sebestova, J. Bendl, S. Khare, R. Chaloupkova, Z. Prokop, J. Brezovsky, D. Baker, J. Damborsky, *PLoS Comput. Biol.* **2015**, *11*, e1004556.
- [36] K.-H. Siu, R. P. Chen, Q. Sun, L. Chen, S.-L. Tsai, W. Chen, *Curr. Opin. Biotechnol.* **2015**, *36*, 98–106.

Manuscript received: August 8, 2017

Accepted manuscript online: August 10, 2017

Version of record online: September 1, 2017
